



Potential existence of anti-postperovskite iron nitride Fe₄N

Samir F. Matar^{a,*}, Gérard Demazeau^a, Naïm Ouaini^b, Alain Largeteau^a

^a CNRS, Université de Bordeaux, ICMCB, 87 avenue Dr Albert Schweitzer, 33600 Pessac, France

^b Université Saint Esprit de Kaslik, Faculté des Sciences et de Génie Informatique, Jounieh, Lebanon

ARTICLE INFO

Article history:

Received 26 February 2010

Accepted 13 April 2010

Available online 27 April 2010

Keywords:

Perovskite

Post-perovskite nitride

DFT

LDA

GGA magnetism

ABSTRACT

The equations of state for cubic anti-perovskite (APV) and hypothetical anti post-perovskite (APPV) forms of Fe₄N obtained within DFT for the spin polarized and non-magnetic configurations, confirm the ferromagnetic ground state of APV-Fe₄N and a non-magnetic one for APPV. The lower equilibrium volume for the latter favors pressure-enabled transition: APV→APPV. Chemical bonding analysis accounting for Fe differentiation into three sublattices for APPV characterized by edge and corner sharing octahedra, leads to a reinforced Fe–N chemical bonding. This is argued to help triggering the pressure transformation. It is the first case of potential post-anti-perovskite nitride.

© 2010 Elsevier Masson SAS. All rights reserved.

1. Introduction

The structural transformations of Minerals in deep Geosphere are an important challenge for explaining the structure and the properties of the Earth [1]. Taking into account that MgSiO₃ and (Mg, Fe) SiO₃ with the perovskite structure are the main components of the lower mantle [2] and due to the seismic anisotropy of the D'' layer at the boundary between the lower mantle and the outer core, the structural transformation of MgSiO₃ was investigated by both Oganov and Ono [3] and Murakami et al. [4]. Both research works postulated the transformation of perovskite (PV) to the CaIrO₃-type structure, called post-perovskite (PPV). The recent stabilization of PPV form for several CaBO₃ oxides, B = Ru [5], Pt [6] and T = Rh [7] extended the interest of the post-perovskite structure from Geosciences to Materials Science. For oxide systems such as CaTO₃ (T = Rh, Pt), we have recently shown [8,9] that the differentiation of the B–O bonds enhances covalence and plays a major role in inducing the PV→PPV transformation. Consequently the PPV structure can be observed for the ABO₃ compositions involving a d⁴ or a d⁵ element and with an A cation such as Ca²⁺.

At the present time, due to the importance of oxides in the Earth mantle, mainly ABO₃ compositions have been investigated. However the PPV form has been observed for NaMgF₃ with the neighborite structure in a pressure range between 28 and 30 GPa by Martin et al. [10]. Such an extension of the PPV structure to non-oxides opens new horizons for the interest of the PPV structure in

materials science. Consequently compounds with this 2D structure having both corner- and edge-sharing octahedra can be characterized by specific electronic properties. The metal-insulator transition observed in Ca_{1-x}Na_xIrO₃ with the PPV structure is an interesting example [11]. Considering the covalence of the B–O bond as a critical factor for stabilizing the PPV structure, nitrides would appear as good candidates for developing novel PPV compounds.

The number of nitrides with the perovskite structure with N occupying O positions in ABO₃, is reduced; ThTa₃N₃ being considered as the most known [12]. However the ferromagnetic nitride, Fe₄N, is well known since its discovery in last century by K. H. Jack [13], both experimentally [14–17] and theoretically [18,19] -and therein cited references. Its formulation, FeNFe₃, leads to assign an anti-perovskite structure in as far as anionic positions are occupied by Fe. Recent high pressure investigations on Fe₄N have pointed out a decrease of magnetic moment due to decreasing volume at room temperature, but no phase transformation was reported [20]. Another work indicates a decomposition of the nitride if temperature is used along with pressure [21]. Consequently it was important to validate through first principles calculations whether the anti – PV → anti – PPV transformation may occur for Fe₄N and what would be the physico-chemical factors triggering it. This is investigated herein within the well established quantum theoretical framework of density functional DFT [22,23].

2. Computational methodology

A pseudo-potential approach within the VASP code [24,25] is used firstly to geometry optimize the nitride and to obtain the

* Corresponding author. Fax: +33 540002761.

E-mail address: s.matar@u-bordeaux1.fr (S.F. Matar).

Table 1

Fe_4N : Lattice coordinates for APV and APPV structures. Starting coordinates for APPV are those of CaRhO_3 [7]. Note that Fe2 and Fe3 are equivalent in APV – $\text{Pm } \bar{3} \text{ m}$

$\text{Fe}_1\text{Fe}_2\text{Fe}_3\text{N}$	APV – $\text{Pm } \bar{3} \text{ m}$	APPV-Cmcm	PPV- CaRhO_3 [7]
Fe1	0,0,0	0, 0.233, $\frac{1}{4}$	Ca : 0, 0.252, $\frac{1}{4}$
Fe2	$\frac{1}{2}$, $\frac{1}{2}$, 0	$\frac{1}{2}$, 0.425, $\frac{1}{4}$	O1: $\frac{1}{2}$, 0.428, $\frac{1}{4}$
Fe3	0, $\frac{1}{2}$, $\frac{1}{2}$; $\frac{1}{2}$, 0, $\frac{1}{2}$	$\frac{1}{2}$, 0.121, 0.029	O2: $\frac{1}{2}$, 0.121, 0.055
N	$\frac{1}{2}$, $\frac{1}{2}$, $\frac{1}{2}$	0,0,0	Rh: 0,0,0

equation of state (EOS) in both non spin polarized (NSP) and spin polarized (SP) magnetic configurations. Besides testing the calculations for their ability to yield the experimental volume of Fe_4N cubic perovskite [13,17], the method enables optimizing the structure and parameters for hypothetical APPV phase, starting from known PPV oxide systems. For initial atomic positions we start from PPV CaRhO_3 by replacing Ca by Fe1, Rh by N and O by Fe2 and Fe3, cf. Table 1. Then the respective equations of states (EOS) are obtained to confront the equilibrium volumes and relative stabilities. This is done through energy-volume curves fitted with Birch EOS [26]. For these purposes, ultra soft pseudo-potentials are used. For the treatment of the effects of exchange and correlation a local density approximation (LDA) [27] has been adopted. Preliminary test calculations for c-PV with gradient functional GGA [28] potentials led to unfavorable total energy with respect to LDA calculations by $\sim 2.8 \text{ eV fu}^{-1}$ while the volumes were found respectively $\sim 2 \text{ \AA}^3$ below and above experimental value. The calculations are converged at energy cut-offs of 500 eV for cubic APV and 347 eV for orthorhombic APPV Fe_4N respectively for the plane-wave basis set. The \mathbf{k} -point integration is carried out with a starting mesh of $4 \times 4 \times 4$ up to $8 \times 8 \times 8$ for best convergence and relaxation to zero strains. The Brillouin-zone integrals are approximated using a special k -point sampling following Blöchl [29].

For a full description of the electronic band structures and of chemical bonding, the scalar relativistic all-electrons augmented spherical wave (ASW) [30,31] method is used. Like in the calculations with pseudo-potentials, the exchange and correlation effects are accounted for with an LDA functional [32]. In the ASW method, the wave function is expanded in atom-centered augmented spherical waves, which are Hankel functions and numerical solutions of Schrödinger's equation, respectively, outside and inside the so-called augmentation spheres. In order to optimize the basis set, additional augmented spherical waves are placed at carefully selected interstitial sites (IS). The choice of these sites as well as the augmentation radii are automatically determined using the sphere-geometry optimization algorithm [33]. Self-consistency is achieved by a highly efficient algorithm for convergence acceleration [34]. The Brillouin zone integrations are performed using the linear tetrahedron method with up to 1728 and 1469 \mathbf{k} -points for cubic and orthorhombic phases respectively [29,31]. In the minimal ASW basis set, we have chosen the outermost shells to represent the valence states using partial waves up to $l_{\text{max}} + 1 = 3$ for Fe and $l_{\text{max}} + 1 = 2$ for N and IS. The completeness of the valence basis set is checked for charge convergence. The self-consistent field calculations are run to a convergence of $\Delta Q = 10^{-8}$ for the charge density and the accuracy of the method is in the range of about 10^{-8} Ryd (1 Ryd = 13.6 eV) regarding energy differences.

The relative magnitude of the chemical bonding is obtained based on the overlap population analysis: S_{ij} , i and j being two chemical species. The crystal orbital overlap population (COOP) [35] criterion is used as implemented within the ASW method [31]. For the purpose of establishing trends of chemical bonding strength, we show the integrated–unitless–COOP (iCOOP): the larger the area below the curves the larger the bonding is. In the

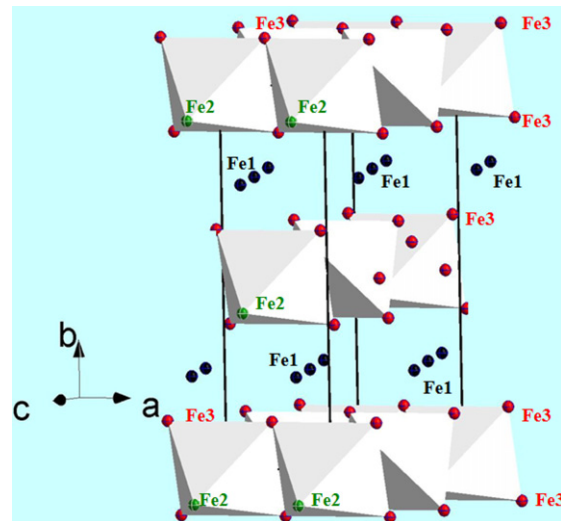


Fig. 1. Schematic view of the corner and edge sharing $N\text{Fe}_2\text{Fe}_3\text{Fe}_4$ octahedra in hypothetical APPV Fe_4N . Nitrogen, at the center of the octahedra, is not observed. (For interpretation of the references to colour in this figure legend, the reader is referred to the web version of this article).

plots positive, negative and zero COOP magnitudes indicate bonding, anti-bonding and non-bonding interactions respectively.

3. Geometry optimization and equation of state

Starting from the internal lattice coordinates of PPV- CaRhO_3 [7] we carried out a geometry optimization for the APPV nitride. The manner of atom replacements is shown in Table 1. For sake of comparison, the APV atomic positions are also presented; these do not change upon geometry relaxation. The resulting coordinates for Fe dispatched into 3 lattice sites, Fe1, Fe2 and Fe3, are seen to slightly depart from those of the oxide while the base centered orthorhombic symmetry within Cmcm space group, is preserved. The resulting APPV nitride structure is shown in Fig. 1. Nitrogen, not seen, is at the center of the $\text{Fe}_2\text{Fe}_3\text{Fe}_4\text{N}$ octahedra which are edge sharing through Fe3. With these coordinates the equilibrium values can be sought from calculations assuming both NSP and SP configurations for both symmetries.

Let us mention here that the calculated total energy pertains to the cohesive energy within the crystal since the solution of the Kohn–Sham DFT equations yield the energy with respect to infinitely separated electrons and nuclei. In as far as the zero of energy depends on the choice of the pseudo-potentials, somehow it becomes arbitrary; i.e. it is shifted but not scaled. However the energy derivatives remain unaltered as well as the equations of state. For this reason one needs to establish the EOS and extract the fit parameters for an assessment of the equilibrium values. This is done from (E, V) set of calculations. The resulting $E = f(V)$ curves are shown in Fig. 2. They have a quadratic variation which can be fitted with Birch equation of state (EOS) to the 3rd order [26]:

$$E(V) = E_0(V_0) + \frac{9}{8}V_0B_0 \left[\left(\frac{V_0}{V} \right)^{\frac{2}{3}} - 1 \right]^2 + \frac{9}{16}B_0(B' - 4)V_0 \left[\left(\frac{V_0}{V} \right)^{\frac{2}{3}} - 1 \right]^3$$

where E_0 , V_0 , B_0 and B' are the equilibrium energy, the volume, the bulk modulus and its pressure derivative, respectively. The fit results are given in Table 2. The expected ferromagnetic (SP) ground state for cubic Fe_4N (Fig. 2a) is identified at a larger volume than assumed non-magnetic (NSP) state [13]. The corresponding SP

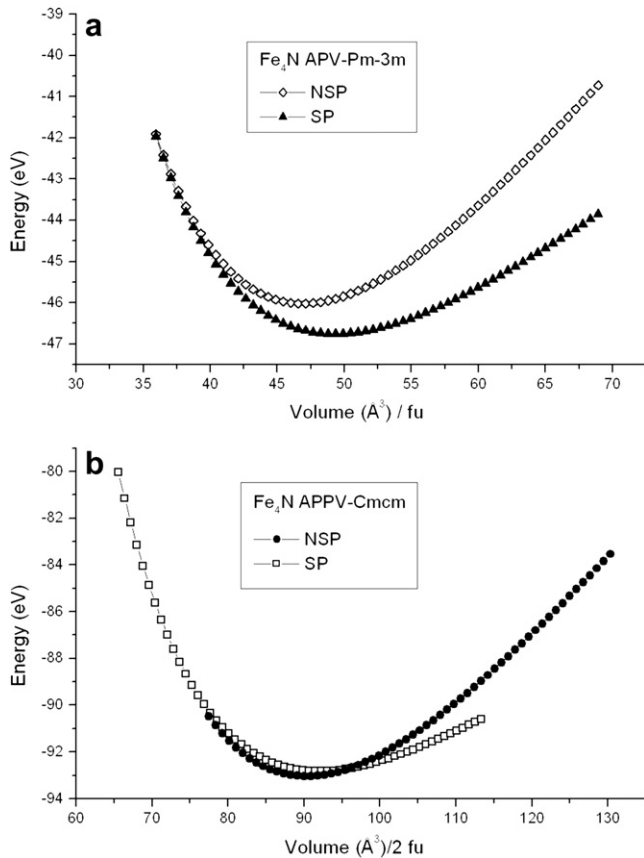


Fig. 2. Fe_4N : Energy versus volume curves for APV (a) and APPV (b) for non-magnetic (NSP) and spin polarized (SP) configurations.

lattice constant of 3.67 \AA is smaller than experimental value (3.87 \AA [13,17]) due to the use of LDA functional based on the homogeneous electron gas distribution. This is accompanied by large energy stabilization by 0.74 eV per f.u. (Table 2) due to magnetic exchange with $M = 6.96 \mu_B$ per fu; this value is in agreement with former works [13,18]. On the contrary, the ground state for hypothetical APPV– Fe_4N is non-magnetic but very close to magnetic polarization. This can be inferred from the small energy stabilization of $\Delta E = 0.1 \text{ eV}$ per fu and from the stabilization of the ferromagnetic case at larger volumes than equilibrium (Fig. 2b) for which the magnetization per fu amounts to $M = 2.23 \mu_B$, i.e. with a much smaller magnitude than in APV. This agrees with experimental finding of a loss of ferromagnetic state with pressure [20] but points out the importance of magnetovolume effects within magnetic nitride systems (cf. ref. [36] and therein cited references).

In both magnetic configurations, the bulk modulus is larger in APPV– Fe_4N versus APV– Fe_4N while being smaller for SP

Table 2

Fe_4N : Fit results from Birch 3rd order equation of state for APV and APPV in both non-spin polarized (NSP) and spin polarized (SP) configurations corresponding to the curves in Fig. 2

$\text{Fe}_1\text{Fe}_2\text{N}$	APV 1 fu		APPV 2 fu	
	NSP	SP	NSP	SP
Energy (eV)	–46.02	–46.76	–93.04	–92.83
Volume (\AA^3)	46.92	49.32	90.32	92.02
Lattice constants (\AA)	3.60	3.67	2.509	2.525
$\frac{b}{a}$			3.86	3.86
			2.96	2.96
Bulk modulus (GPa)	322	228	337	240

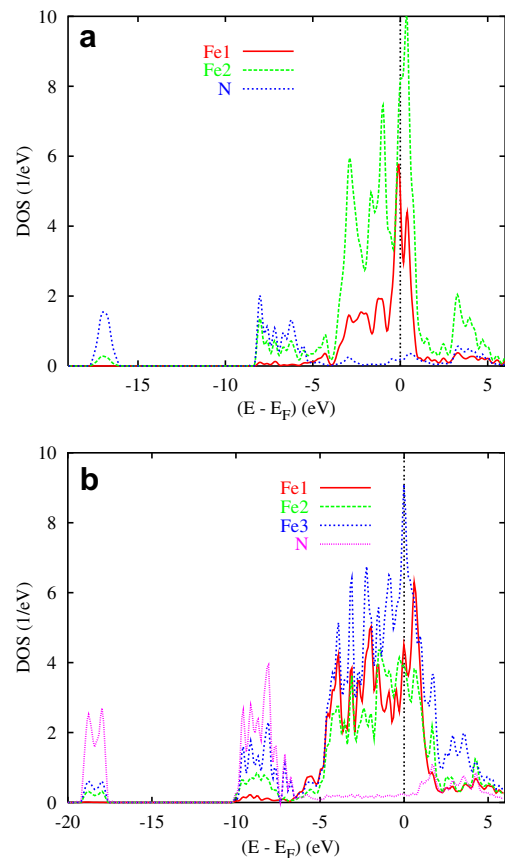


Fig. 3. NSP Fe_4N : Site projected density of states for APV (a) and APPV (b). (For interpretation of the references to colour in this figure legend, the reader is referred to the web version of this article).

configuration in each phase due to the higher compressibility of the magnetic state. This is concomitant with smaller volume for APPV– Fe_4N and lets suggest that this phase could be obtained by applying pressure. The larger B_0 values for APPV for both NSP and SP, are likely due to the improved compactness of the octahedra within the layer, in as far as they are assembled into corner as well as edge sharing motifs in APPV phase. In other words the system should present a larger incompressibility within the layers than between them so that the average incompressibility is higher. In both varieties, the magnitude of B' amounts to 4, a value usually encountered [38].

4. Electronic structure and chemical bonding

Using the equilibrium values of equilibrium ground states (Table 2) we calculate the electronic structures and the properties of chemical bonding for both forms. While extensive results on the magnetic structure both from experiment and theory for APV– Fe_4N are available [13,17–19,36,37], we focus here on the site projected DOS and chemical bonding of the non-magnetic configuration.

4.1. Density of states

At self-consistent convergence, charge transfer is observed from Fe and N towards IS with amounts of ~ 0.5 – 1 electron. These transfers are not meaningful of an ionic character such as N^{3-} , not encountered in such calculations on one hand and they point to a covalently bonded nitride system on the other hand.

The site projected density of states (DOS) are shown at Fig. 3; energy reference along the x axis is with respect to the Fermi level

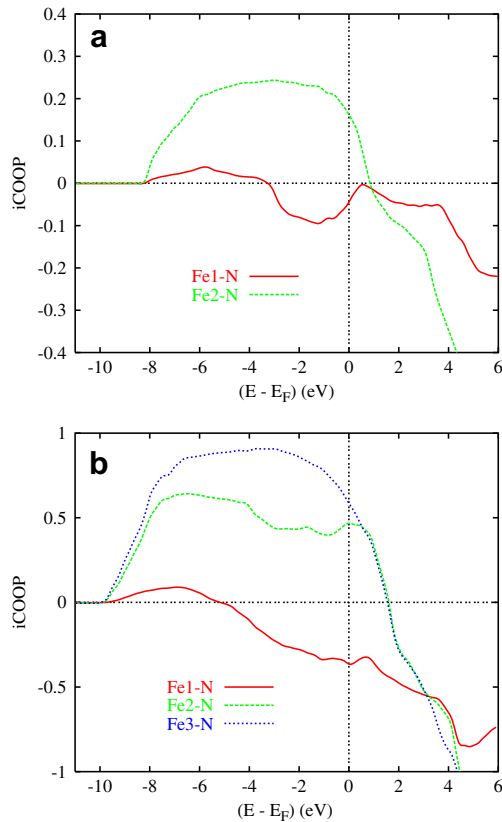


Fig. 4. NSP Fe_4N : Chemical bonding from integrated COOP for Fe–N interactions in APV (a) and APPV (b). (For interpretation of the references to colour in this figure legend, the reader is referred to the web version of this article).

(E_F). Due to a twice larger APPV unit cell with respect to APV one, the DOS (y-axis) are twice larger in Fig. 3b versus Fig. 3a. Both systems are characterized by a metallic behavior in such a spin degenerate magnetic configuration with a large contribution from Fe sites. In the mean field Stoner theory of band ferromagnetism [39] this is indicative of an instability of the system in such a spin degenerate configuration and that spin polarization should occur on Fe sites as mentioned above. The lower part of the valence band is dominated by nitrogen s states which have similar shape to Fe. The N-p states are found around -10 eV with same shape as Fe PDOS, whence the bonding between them. The Fe-d states at the Fermi level are of non-bonding nature; their main contribution is in the onset of the magnetic moment.

4.2. Chemical bonding

The DOS results can be further assessed in a chemical bonding qualitative analysis. Focussing on the bonding between the iron different sites with nitrogen, we show the integrated – unitless – COOP (*iCOOP*) in Fig. 4. The larger the area below the curves the larger the bonding is. For the purpose of enabling comparison in magnitude, the same number of atoms is taken for a given Fe–N interaction, i.e. 1:1 for APV and 2:2 for APPV. In the cubic APV, the difference of *iCOOP* magnitudes arises from distance criteria because $d(\text{Fe1–N}) = a\sqrt{3}/2$ while $d(\text{Fe2–N}) = a/2$ leading to stronger bonding for the latter. However when the relative bonding strengths are examined in APPV, and considering the distances; $d(\text{Fe1–N}) \sim 2.9 \text{ \AA}$, $d(\text{Fe2–N}) \sim 1.9 \text{ \AA}$ and $d(\text{Fe3–N}) \sim 1.8 \text{ \AA}$, the distance criterion is found responsible of difference for (Fe1–N) versus (Fe2–N) and (Fe3–N) *iCOOP* areas, i.e. the larger the

interatomic spacing, the weaker the bonding. But interatomic separation is not sufficient to explain the changes in bonding between (Fe2–N) and (Fe3–N). It can be argued that the enhanced covalence of Fe3–N due to the edge sharing $\text{Fe}_2\text{Fe}_3\text{N}$ octahedra through Fe3 should be at the origin of the difference. This is a new feature brought by the post-perovskite structure. It can also be invoked to explain the relative hardening of the system in this structure (cf. Table 2).

5. Conclusion

Using theoretical modeling tools within DFT, the equations of state (EOS) of anti-perovskite and anti-post-perovskite Fe_4N were established in both spin degenerate and spin polarized configurations. In agreement with experimental and theoretical literature, the ferromagnetic ground state is found for ambient phase at smaller volume for anti-perovskite while the ground state for anti-post-perovskite Fe_4N is non-magnetic. Its smaller volume suggests a pressure-enabled transition: APV \rightarrow APPV which is helped by a change of the nature of the chemical bonding due to the increased covalence within anti-post-perovskite, characterized by corner as well as edge sharing Fe_6N octahedra contrary to only corner sharing octahedra known for the perovskite structure. It is an original proposition of an anti-post-perovskite structure chemical system. The stabilization of a high pressure form of Fe_4N with the anti-post-perovskite structure in the low mantle could be a possible way for the sequestration of nitrogen in the earth.

Acknowledgements

Computational facilities were provided by MCIA (Mésocentre de Calcul Intensif en Aquitaine), Université de Bordeaux.

References

- [1] D. Yu. Pushcharovsky, R. Oganov, Structural transformations of minerals in deep geospheres: a review. *Crystallogr. Rep.* 51 (2006) 767.
- [2] G. Fiquet, *Z. Krist.* 216 (2001) 248.
- [3] A.R. Oganov, S. Ono, *Nature* 430 (2004) 445.
- [4] M. Murakami, K. Hirose, K. Kawamura, N. Sata, Y. Ohishi, *Science* 304 (2004) 855.
- [5] H. Kojitani, Y. Shirako, M. Akaogi, *Phys. Earth. Planetary. Interiors.* 165 (2007) 127.
- [6] Y. Inaguma, I. K-Hasumi, M. Yishida, T. Ohba, T. Katsumata, *Inorg. Chem.* 47 (2008) 1868.
- [7] Y. Shirako, H. Kojitani, M. Akaogi, K. Yamaura, E. Takayama-Muromachi, *Phys. Chem. Minerals* 36 (2009) 455.
- [8] S.F. Matar, G. Demazeau, A. Largeau, *Solid. State. Sci.* 12 (2010) 373.
- [9] S.F. Matar, G. Demazeau, A. Largeau, *Chem. Phys.* 352 (2008) 92.
- [10] C.D. Martin, Y. Meng, V. Prakapenka, J.B. Parise, *J. Appl. Crystallogr.* 41 (2008) 38.
- [11] K. Ohgushi, Y. Matsushita, N. Miyajima, Y. Katsuya, M. Tanaka, F. Izumi, H. Gotou, Y. Ueda, T. Yagi, *Phys. Chem. Minerals* 35 (2008) 189.
- [12] N.E. Brese, F.J. DiSalvo, *J. Solid. State. Chem.* 128 (1995) 378.
- [13] K.H. Jack, *Proc. R. Soc. Lon* A11 (1948) 34.
- [14] K. Tagawa, E. Kita, A. Tasaki, *Jpn. J. Appl. Phys.* 21 (1982) 1596.
- [15] S. Matar, G. Demazeau, B. Siberchicot, *IEEE. Trans. Magnetics.* 26 (1990) 60.
- [16] B. Siberchicot, S. Matar, L. Fournès, G. Demazeau, *J. Solid. State. Chem.* 84 (1990) 10.
- [17] K.H. Jack, *J. Appl. Phys.* 76 (1994) 6620.
- [18] S. Matar, G. Demazeau, *J. Phys. France.* IV. 2 (1992) C3.
- [19] B. Siberchicot, *J. Magn. Magn. Mater.* 321 (2009) 3422.
- [20] N. Ishimatsu, H. Marutama, N. Kawamura, M. Suzuki, Y. Ohishi, M. Ito, S. Nasu, T. Kawakami, O. Shimomura, *J. Phys. Soc. Jpn.* 72 (2003) 2372.
- [21] R. Niewa, D. Rau, A. Wosylus, K. Meier, M. Wessel, M. Hanfland, R. Dronskowski, U. Schwarz, *J. Alloys. Compounds.* 480 (2009) 76.
- [22] P. Hohenberg, W. Kohn, *Phys. Rev. B* 136 (1964) 864.
- [23] W. Kohn, L.J. Sham, *Phys. Rev. A* 140 (1965) 1133.
- [24] G. Kresse, J. Furthmüller, *Phys. Rev. B* 54 (1996) 11169.
- [25] G. Kresse, J. Joubert, *Phys. Rev. B* 59 (1999) 1758.
- [26] F. Birch, *J. Geophys. Res.* 83 (1978) 1257.
- [27] D.M. Ceperley, B.J. Alder, *Phys. Rev. Lett.* 45 (1980) 566.
- [28] J.P. Perdew, S. Burke, M. Ernzerhof, *Phys. Rev. Lett.* 77 (1996) 3865.
- [29] P.E. Blöchl, *Phys. Rev. B* 50 (1994) 17953.

- [30] A.R. Williams, J. Kübler, C.D. Gelatt, *Phys. Rev. B* 19 (1979) 6094.
- [31] V. Eyert, *The Augmented Spherical Wave Method – a Comprehensive Treatment*, *Lect. Notes Phys.* 719. Springer, Berlin Heidelberg, 2007.
- [32] S.H. Vosko, L. Wilk, M. Nusair, *Can. J. Phys.* 58 (1980) 1200.
- [33] V. Eyert, K.-H. Höck, *Phys. Rev. B* 57 (1998) 12727.
- [34] V. Eyert, *J. Comput. Phys.* 124 (1996) 271.
- [35] R. Hoffmann, *Angew. Chem. Int. Ed. Engl.* 26 (1987) 846.
- [36] P. Mohn, S.F. Matar, *J. Magn. Magn. Mater.* 191 (1999) 234.
- [37] S.F. Matar, *J. Alloys Comp.* 345 (2002) 72.
- [38] S. Stølen, R. Trønnes, *Phys. Earth. Planetary. Interiors.* 164 (2007) 50.
- [39] P. Mohn, *Magnetism in the Solid State – an Introduction Solid-State Sciences*, In: *Springer Series*. Springer, Heidelberg, 2003.